Chemical evolution of atmospheric organic carbon over multiple generations of oxidation

Gabriel Isaacman-VanWertz[1,2]*, Paola Massoli[3], Rachel O'Brien[1], Christopher Lim[1], Jonathan P. Franklin[1], Joshua A. Moss[1], James F. Hunter[1], John B. Nowak[3,#], Manjula R. Canagaratna[3], Pawel K. Misztal[4], Caleb Arata[4], Joseph R. Roscioli[3], Scott T. Herndon[3], Timothy B. Onasch[3], Andrew T. Lambe[3], John T. Jayne[3], Luping Su[5], Daniel A. Knopf[5], Allen H. Goldstein[4], Douglas R. Worsnop[3], Jesse H. Kroll[1]*

[1]Department of Civil and Environmental Engineering, Massachusetts Institute of Technology, Cambridge, Massachusetts 02139, USA

[2]Department of Civil and Environmental Engineering, Virginia Tech, Blacksburg, Virginia 24061, USA

[3]Aerodyne Research Inc., Billerica, Massachusetts 01821, USA

[4]Department of Environmental Science, Policy, and Management, University of California, Berkeley, California 94720, USA

[5]School of Marine and Atmospheric Sciences, Stony Brook University, Stony Brook, New York 11794, USA

[#]Now at NASA Langley Research Center, Hampton, VA 23681, USA

Abstract

The evolution of atmospheric organic carbon (OC) as it undergoes oxidation has a controlling influence on concentrations of key atmospheric species, including particulate matter, ozone, and oxidants. However, the full characterization of OC over hours to days of atmospheric processing has been stymied by its extreme chemical complexity. Here we study the multigenerational oxidation of α-pinene in the laboratory, characterizing products with several state-of-the-art analytical techniques. While quantification of some early-generation products remains elusive, full carbon closure is achieved (within uncertainty) by the end of the experiments. This enables new insights into the effects of oxidation on OC properties (volatility, oxidation state, and reactivity), and the atmospheric lifecycle of OC. Following an initial period characterized by functionalization reactions and particle growth, fragmentation reactions dominate, forming smaller species. After approximately one day of atmospheric aging, most carbon is sequestered in two long-lived reservoirs, volatile oxidized gases and low-volatility particulate matter.

Organic compounds play a central role in the chemistry of the atmosphere, by contributing to ozone formation,[1,2] serving as the primary sink for oxidants in the atmosphere,[3,4] and constituting a substantial fraction of global submicron particulate matter.[5,6] Organic carbon (OC) enters the atmosphere primarily as high-volatility gases. Oxidation of these compounds yields a large number of products, including organic species in the gas phase (gas-phase OC, gOC), organic species in the condensed phase (particle-phase OC, pOC), and inorganic carbon-containing species (CO and CO_2). All of these products (other than CO_2) may themselves undergo further oxidation, continuing this process over multiple generations to produce a highly complex, chemically dynamic mixture of compounds that spans a wide range in chemical composition and properties (e.g., volatility).[7–11] Oxidation continues until OC is either converted to CO_2, or removed from the atmosphere through deposition to the Earth's surface, thereby transporting a wide range of organic compounds into other components of the Earth system. Our ability to track the oxidative evolution of OC over its entire atmospheric lifetime therefore controls not only our ability to understand critical issues in air quality and atmospheric chemistry, but ultimately to understand the impacts of organic emissions on human health, ecosystems, and Earth's climate.

The comprehensive measurement of all oxidation products from a given chemical system has been elusive due to the analytical challenges associated with detecting, characterizing, and quantifying compounds within complex organic mixtures. Only studies of the simplest organic compounds have achieved "carbon closure," fully characterizing the product mixture throughout oxidation.[12] For larger species, a large fraction of the products has remained unmeasured and/or uncharacterized, even in the early stages of reaction (first 1-2 generations of oxidation).[13,14] As a result, there is substantial uncertainty as to the fate and impact of OC over timescales longer than several hours after emission. For example, the possibility of substantial unmeasured "pools" of OC has major implications for the formation of particle-phase mass through the gas-to-particle partitioning of condensable gases. It has traditionally been assumed that such unmeasured carbon will not condense to contribute to particle-phase mass. However, if instead unmeasured carbon in experiments is irreversibly lost to chamber walls via vapor deposition[15] before reacting to form lower-volatility gases or oxidizes to form low-volatility species over multiple generations not typically accessed in laboratory studies,[9,16] then formation of pOC from many precursors may be substantially higher than understood. The properties and reactivity of organic oxidation products formed over multiple generations will also impact ozone production, removal pathways (e.g. wet and dry deposition) of pollutants, and reactivity and cycling of oxidants. A quantitative, predictive description of these processes across all spatial scales relies critically on the measurement of the chemistry of such species, and more generally on our ability to measure and track all OC in a reactive system.

Here we apply recent advances in analytical instrumentation to characterize the full mixture of products formed in hydrocarbon oxidation with the goal of achieving "carbon closure," enabling a more complete understanding of the chemical properties and transformation processes of atmospheric OC. We access the entire range of expected chemical properties of suspended products[17] with an array of state-of-the-art analytical instruments: an aerosol mass spectrometer[18] (AMS) and scanning mobility particle sizer (SMPS) to measure pOC, a proton transfer reaction mass spectrometer[19,20] (PTR-MS) and two chemical ionization mass spectrometers[21] (I^- CIMS and NO_3^- CIMS[22–25]) to measure gOC, and two tunable infrared laser differential absorption spectrometers (TILDAS) to measure C_1 compounds (CO, formaldehyde, and formic acid). We combine the data from these instruments to present a unified, time-resolved description of the chemical composition of two oxidation systems: initial oxidation of α-pinene (a

monoterpene) through photo-oxidation by hydroxyl radicals (OH) in the presence of NO, and ozonolysis in the absence of NO, followed in both cases by continued high-NO OH oxidation. See Methods and Supplementary Information Section S1 for details on instrument operation and reaction conditions. These systems were chosen because their initial chemistry has been subject to extensive theoretical and experimental characterization,[26–30] but the subsequent multi-generational oxidation ("aging") of the reaction mixture (particularly gOC) has received substantially less study.[31] By the end of the experiments, all carbon is measured to within uncertainty, enabling a coherent and detailed picture of the chemical evolution of the product mixture, and providing new insights into the lifecycle and fate of atmospheric OC.

Results

Carbon closure

All products measured in the OH-initiated oxidation of α-pinene are shown in Figure 1. Results are qualitatively similar to those in the ozonolysis experiment, so those results are given in the Supplementary Information (Figure S1). Initial reaction of α-pinene is immediately accompanied by a concomitant rise in oxidation products in both gOC and pOC. Particle-phase OC is formed in the first generations of oxidation, with only minor additional formation after the α-pinene is fully consumed, and accounts for 14±3% of the total carbon by the end of the experiment (~24 hours of equivalent atmospheric oxidation). Identified gas-phase products include CO, formaldehyde, formic acid, acetic acid, acetone, and pinonaldehyde (identified as described in Supplementary Information Section S5). Concentrations of each identified product vary over the course of the experiment, but in total account for 41±5% of the carbon by the end. CO_2 is not measured here but is expected to be similar in concentration to CO (~4%).[32]

In addition to known compounds, there are a large number of ions (370) in the PTR-MS and I^- CIMS mass spectra for which molecular formulas are known but structures cannot be unambiguously assigned. These "unidentified ions" are treated as gas-phase species of the known molecular formula. The dominant contributor is $C_3H_4O_4$ (yield of ~5%), which has previously been observed in the atmosphere and identified as malonic acid;[33,34] however, its ion cluster strength (Figure S4a) indicates that it is not malonic acid but rather some isomer thereof (highlighting the difficulty in assigning identities to ions based only on their molecular formula). Species measured by the NO_3^- CIMS (extremely low volatility, highly oxidized gases)[35] account for <0.5% of the total carbon (Figure S3), so are not shown in Figure 1. Together unassigned species comprise $47\pm^{17}_{20}\%$ of the carbon at the end of the experiment. Less than 20 ppbC (4% of carbon) is from ions with molecular formulas detected by multiple instruments, so instrument overlap has little effect on total carbon accounting.

The total measured carbon yield is 102% by the end of the experiment. Uncertainty (1σ) is -22/+30%, and dominated by uncertainty in quantification of lightly functionalized oxidized gases, which may be reducible in future work to ±20% (see Supplementary Information Section S4 for details). Thus, "carbon closure" is achieved in this experiment within instrument uncertainties, demonstrating that the suite of instruments allows for complete quantification and characterization of reaction products formed over these timescales. This also indicates that the loss of condensable carbon to chamber walls or other surfaces is not a major sink for reaction products in this experiment, as expected given the fast rate of oxidation and the use of seed particles as a condensation sink,[36–38] and supported by modeled gas-particle-wall partitioning (Supplementary Information Section S6).

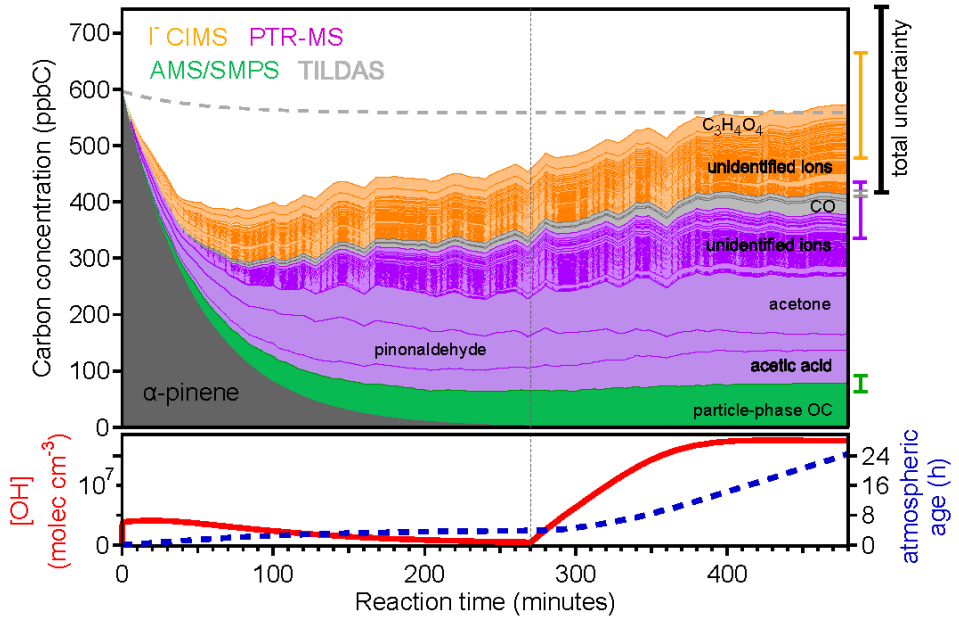

Figure 1. Measured species throughout the photo-oxidation of α-pinene (dark gray) in the presence of NO. Each product ion is colored by the instrument by which it was measured (green: AMS/SMPS, purple: PTR-MS, light gray: TILDAS, orange: I^- CIMS). Unlabeled species measured by TILDAS are formic acid and formaldehyde. Uncertainty range for each instrument shown on right. Total expected carbon in the system (after accounting for dilution of the precursor) shown as light gray dashed line at ~550 ppbC. All concentrations are corrected for dilution; pOC is also corrected for particle deposition to the chamber walls. Bottom panel: modeled OH concentration (red line) and approximate photochemical age in the atmosphere (blue dashed line), assuming an average OH concentration of 2×10^6 molec cm^{-3}. The corresponding plot for the α-pinene ozonolysis experiment is given in Figure S1.

Not all carbon is measured throughout the entire experiment, however, with some "missing" carbon (up to ~40%) left unmeasured early in the experiment. The time dependence of this unmeasured carbon suggests it is made up of early-generation products that quickly react away (with a ~4h timescale) to yield measured products, leading to the observed carbon closure by the end of the experiment. These unmeasured species may be compounds that are not readily detected by the instrument suite. For example, the one peak in the I^- CIMS mass spectrum that is above the detection limit but substantially below the threshold for reliable instrument calibration (and hence not included in Figure 1) is $C_{10}H_{17}NO_4$ (Figure S5). This likely corresponds to α-pinene hydroxynitrate, a first-generation oxidation product known to be formed in high yields (~15%), but that is not sensitively measured by any of the present instruments.[28,39] Importantly, the temporal behavior and ion intensity of this species (after applying an approximate calibration factor[40]) matches the unmeasured carbon well (Figure S10). Since "missing" carbon is also observed in the ozonolysis experiment (Figure S1), for which no nitrate formation is expected, the poor sensitivity of this instrument suite to lightly-oxidized, lower-volatility gases (Supplementary Information Section S7) leads to poor carbon closure in the early generations of oxidation. In addition, these compounds may reversibly partition to reactor or inlet walls (Figure S9) and re-volatilize upon reaction of their gas-phase component with OH, which could also contribute to unmeasured carbon early in the experiment (Figure S10). Thus, despite uncertainties related to its molecular identity, the unmeasured carbon is likely comprised of lightly oxidized, intermediate-volatility, early-generation products. Moreover, the majority of the OC (and all of it by the end of the experiment)

is fully quantified and chemically characterized, providing a unique opportunity to examine the evolution of the composition and chemistry of OC over multiple generations of oxidation.

Evolving properties of the carbon

The changing composition of this complex mixture with oxidation is shown in Figure 2, as three "snapshots" of the product distribution, shown in "two-dimensional volatility basis set" space (carbon oxidation state, OS_C, vs. volatility, expressed as saturation concentration, c^*).[41,42] Suspended carbon in the first hour of the experiment (panel a) is dominated by the precursor, α-pinene, and the formation of products with intermediate volatility ($c^* = 10^3$-10^6 μg m^{-3}), as well as some higher-volatility gases (e.g., acetone, acetic acid), and particle-phase mass. By the end of the initial oxidation, after nearly all α-pinene has reacted (panel b), the product mixture spans a wide range of volatilities and oxidation states. Upon further oxidation (panel c), the distribution of products changes further, indicating the importance of continuing oxidation chemistry beyond the initial α-pinene oxidation.

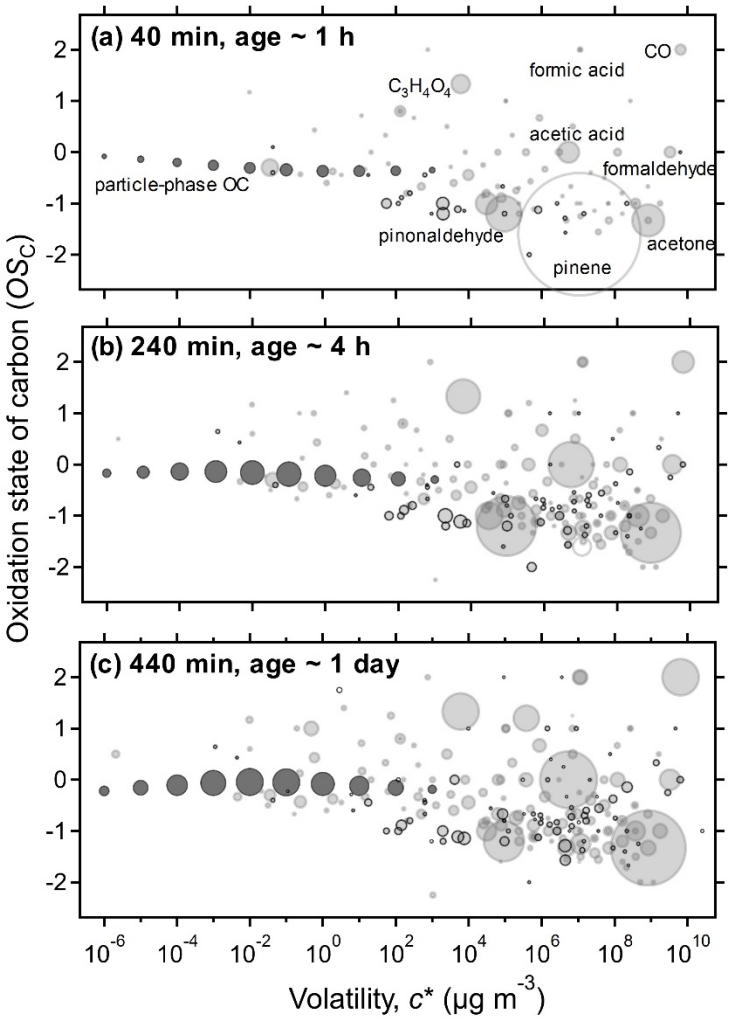

Figure 2. Distribution of measured carbon across in the OS_C-vs-c^* chemical space. Circle area is proportional to carbon concentration. Hollow: α-pinene, light gray: gas-phase species, dark gray: pOC, shown at average OS_C of each volatility bin. Gas-phase species containing nitrate groups (defined as containing nitrogen and ≥3 oxygen

atoms) are outlined. Distributions are provided after approximately (**a**) 1 hour, (**b**) 4 hours, and (**c**) 24 hours of equivalent atmospheric age. The full time evolution of these data is available as a video in the Supplementary Information online.

In this chemically dynamic system, the behavior of different products is determined by their formation pathways as well as their lifetime versus further oxidation by OH. Some early-generation products, including most IVOCs (e.g., pinonaldehyde and multi-functional nitrates), exhibit rapid decreases in concentration after formation, consistent with their high reactivity.[43,44] By contrast, concentrations of some of the volatile compounds (e.g., CO and acetone) consistently increase throughout the experiment. These are formed both from the initial oxidation of α-pinene (panel a) as well as from the multigenerational oxidation of reaction products (panel c), and their slow reaction rates with OH preclude any significant decay over the timescales of the experiment. This category of less-reactive products also includes pOC, which increases throughout the experiment with only relatively minor changes in average properties, consistent with the long lifetime of particulate carbon against heterogeneous oxidation by gas-phase oxidants.[45,46]

The evolution of the organic mixture as a whole can be described in terms of changes to key chemical properties of the measured products. Figure 3 shows the evolving distributions of three such properties: carbon number (n_C), OS_C, and c^*. The n_C of observed products (Figure 3a) exhibits a clear and dramatic change with oxidation: C_{10} species make up a large fraction (~50%, likely an underestimate since the early-generation unmeasured species are likely C_{10}), indicating the importance of functionalization reactions (addition of oxygen-containing groups) early in the reaction, as well as their contribution to pOC formation. However further oxidation depletes the C_{10} compounds, which account for only 12% of the carbon by the end of the experiment. Their oxidation produces species with smaller carbon numbers (in particular $C_{1\text{-}3}$), suggesting that later-generation oxidation is dominated by fragmentation reactions. The OS_c distribution of the product mixture (Figure 3b) is initially dominated by species with low (<-0.5) oxidation states, but further oxidation leads to the formation of higher oxidation state products, including very oxidized products with oxidation state >+1 (e.g. formic acid and CO) and a few less-oxidized species (mostly acetone). The volatility distribution (Figure 3c) also undergoes major changes, with initial products dominated by IVOCs, C_{10} products formed by the addition of 1-3 functional groups to the carbon skeleton of the precursor. However, as these species oxidize and fragment, the distribution of volatilities shifts away from IVOCs, toward both higher- and lower-volatility products. By the end of the experiment, IVOCs represent a small fraction of the total carbon, which is instead dominated by high-volatility gases (formed from fragmentation reactions) or pOC (formed mostly from functionalization reactions). The trends observed in Figure 3 are further enhanced by including α-pinene (Figure S2) or unmeasured species, as those have similar chemical properties as early-generation products (large, moderately volatile, and lightly oxidized). The ozonolysis experiment (Figure S1) exhibits the same trends as the OH experiment, only with fewer changes during the initial oxidation, since the reaction ceases after the oxidation of the double bonds.

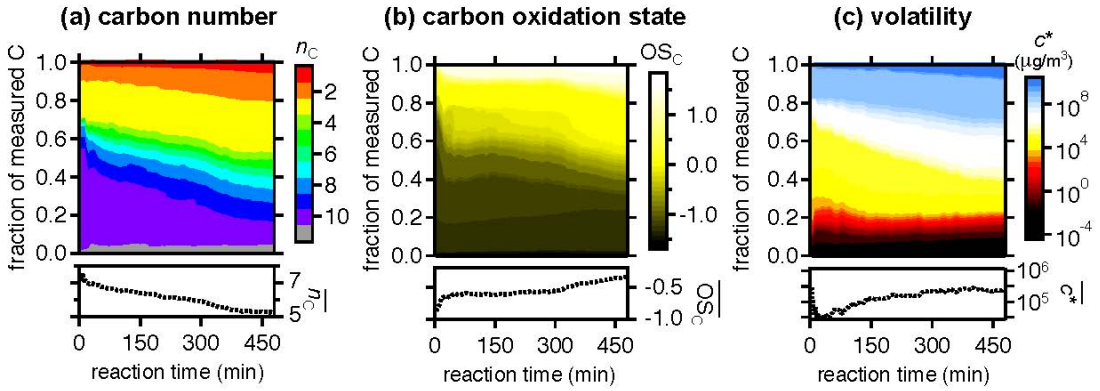

Figure 3. Evolution of the chemical properties of gas- and particle-phase products from α-pinene photo-oxidation, shown as time-dependent distributions of total measured carbon. The properties of only the oxidation products (and not of the α-pinene precursor) are shown; the plots in which α-pinene is included is provided in Figure S2. Properties shown are (**a**) number of carbon atoms, n_C, (**b**) oxidation state of carbon, OS_C, and (**c**) volatility in terms of saturation concentration, c^*, each denoted by the color scale shown. Trends in the carbon-weighted average of each property are shown in bottom panels.

The evolution of the organic mixture, in which the early-generation species (mostly large, lightly-oxidized, intermediate volatility species) react to form small, volatile species in the gas phase and low-volatility species in the particle phase, has important implications for the evolving reactivity and lifetime of atmospheric OC. Figure 4a shows the changes to the distribution of the atmospheric lifetime against reaction with OH (τ_{ox}) of the product mixture; unlike Figure 3, this includes unmeasured species, since their lifetime can be directly estimated from their observed rate of decay (see Figure S10). The lifetimes of the initial products are generally short. Functionalized IVOCs have lifetimes of only a few hours,[45] so observation of a similar lifetime (~4 hours) for the unmeasured carbon further supports its assignment as reactive IVOCs. However some of the other products are extremely long-lived with respect to OH oxidation, such as CO (τ_{ox} = 39 days[47]), acetone (τ_{ox} = 34 days[48]), and pOC (τ_{ox} = 69 days[46]). Over the course of the experiment, the IVOCs react away and these longer-lived species continue to grow in, increasing the average lifetime of products in the mixture from 5 hours to 2 days. By the end of the experiment, more than half of the carbon is in species that are sufficiently long-lived (τ_{ox} > 20 hrs) to be unreactive on the timescale of the experiment. This tendency toward long-lived species is a natural consequence of any multigenerational reaction system, since less-reactive products represent "kinetic bottlenecks" and hence will necessarily accumulate. In the present system, this tendency is closely correlated with the evolving volatility distributions, since long-lived species tend either to be small gas-phase oxygenates (e.g., CO, acetone), or present in the condensed phase (as pOC). Thus, within approximately a day of atmospheric aging, the volatility distribution of the product mixture is bimodal, dominated by particles and long-lived high-volatility gases (Figure 4b). This decrease in reactivity through sequestration of carbon in "low-reactivity pools" occurs roughly exponentially, with a characteristic time of ~3 hours (Figure 4c); this timescale matches the lifetime of the first-generation products that drive the initial reactivity of the product mixture.

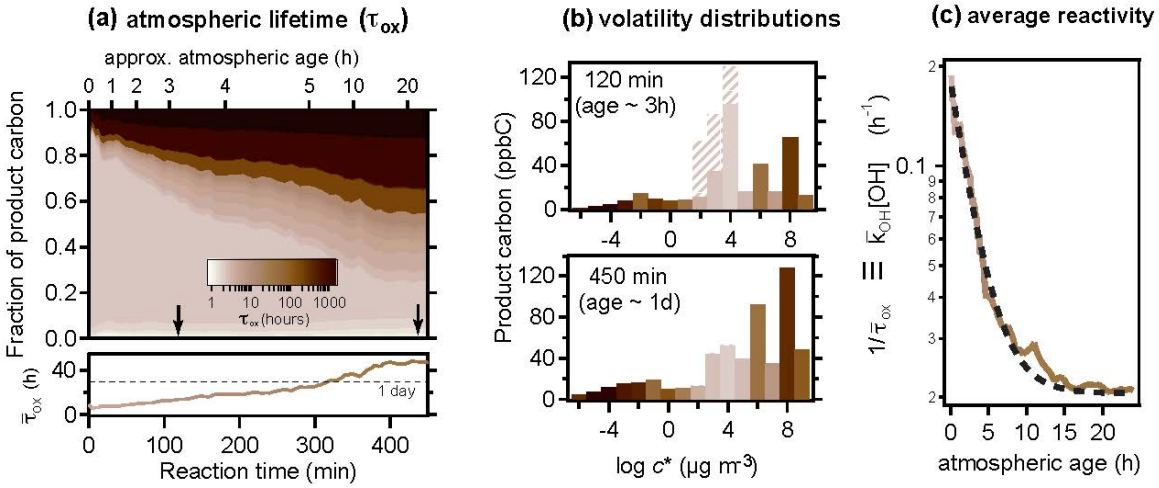

Figure 4. Evolution of atmospheric lifetime against oxidation by OH (τ_{ox}) and its impacts. (**a**) Time-dependent distribution of τ_{ox} including unmeasured carbon (for which τ_{ox} = 4 h) and (bottom panel) time-dependent trends in the carbon-weighted average τ_{ox}. (**b**) Volatility distribution of carbon at two points in the experiment, denoted by arrows in panel (a), relatively early (top) and late (bottom) in the reaction. Volatility bins are colored by τ_{ox} with the same color scale as in panel a. Unmeasured carbon is assumed to be distributed evenly across c^*= 10^2-10^4 μg m^{-3} (hashed bars) for illustrative purposes. (**c**) Carbon-weighted average OH reactivity (assuming average OH concentration of 2×10^6 molec cm^{-3}). Exponential fit (black dashed line) has a decay constant, $\tau_{\overline{k_{OH}}}$, of 2.8 hours.

Discussion

By characterizing all the products formed in a complex oxidation system, we have demonstrated that atmospheric OC evolves through multi-generational oxidation to become sequestered in long-lived reservoirs of volatile gases and low-volatility particles. Initial oxidation occurs through the addition of functional groups to form pOC mass and large, intermediate-volatility gases, but upon further oxidation gas-phase products quickly fragment into high-volatility compounds. Particulate carbon and some oxidized volatile gases are resistant to further oxidation by OH, so carbon effectively becomes sequestered in these two pools. The present results data are limited to the oxidation of a single precursor hydrocarbon, under a limited set of reaction conditions, and other chemical systems may exhibit somewhat different behavior. However, known long-lived products (e.g., pOC, formic acid, CO, etc.) are formed by a wide range of oxidation systems, and longer-lived species will necessarily accumulate over the course of multiple generations of oxidation. Thus the general trends shown in Fig 4 – the eventual decrease in reactivity and the bifurcation in volatility – are likely to be common features of the oxidation of most atmospheric organic species.

The observed timescale for oxidative removal of reactive gases and formation of long-lived species has broad implications for understanding the fate of atmospheric OC on global and regional scales. Near emission sources, the diverse and complex mixture of functionalized gases formed from emissions are likely to comprise a significant fraction of suspended carbon, playing a critical role in particle growth, OH reactivity, and depositional loss.[11,16,49–53] However, farther from emissions, IVOCs will be substantially depleted and most mass will be comprised of relatively few long-lived constituents, so composition and removal of OC in remote regions will be dominated by particles and $C_{1\text{-}3}$ gases. Where an airmass is on the continuum between near- and far-field is a function of both the inherent timescales for oxidation of a given chemical system and the "average age" of the OC. Some approaches to quantify the average age

of an airmass have been developed, but are generally limited to anthropogenically-influenced chemistries.[54,55] The oxidation processes studied here compete with wet and dry deposition to determine the fate of atmospheric OC. The relative timescales of each govern the extent to which emitted carbon is deposited as lightly-functionalized species before being sequestered by oxidation. The timescales of oxidation measured in this work need to be complemented by better observational constraints on average age of OC and timescales of removal in order to improve understanding of the lifecycle and fate or OC under a range of atmospheric conditions.

Methods

Reaction conditions

Studies were carried out using a fixed-volume temperature-controlled 7.5 m^3 Teflon environmental chamber in which was mixed α-pinene (60 ppb), ammonium sulfate aerosol (~70 μg m^{-3}), and a non-reactive tracer used to measure dilution rate (hexafluorobenzene). Oxidant was introduced as HONO (50 ppb) in the presence of ultraviolet light (300-400 nm) to produce OH radicals, or ozone (~350 ppb). Multi-generational oxidation occurred through the introduction of ~2 ppb/min HONO in the presence of ultraviolet light. All data are corrected for dilution due to instrument sampling. Reported particle mass concentration is corrected for loss to the walls using a rate calculated from the loss rate of seed particles prior to reaction. Additional details provided in the Supplementary Information Section S1.

Measurements

Four high-resolution (m/Δm ≈ 4000) time-of-flight mass spectrometers (HTOF; Tofwerk AG) were used in this work: PTR-MS[19,20] (Ionikon Analytik), two CIMS[21] (Aerodyne Research Inc.) using I^- and NO_3^- as reagent ions,[22–25] and an AMS[18] (Aerodyne Research Inc.). The latter sampled downstream of a ThermalDenuder[57] to measure volatility distribution of particles. Two TILDAS[58] (Aerodyne Research Inc.) instruments measured C_1 compounds. Particle-phase composition was measured by the I^- CIMS using a "FIGAERO" inlet.[59] Particle size distributions measured by Scanning Mobility Particle Sizer (TSI Inc.) was converted to mass concentration by an assumed density. Detailed operation conditions and calibration methods are provided for all instruments in the Supplementary Information Section S1. Calibration and data analysis was performed where possible through previously published techniques and with commercially available software. Detailed information regarding the comprehensive calibration of I^- CIMS data, and identification and quantification of known species in PTR-MS data are described in the Supplementary Information Sections S4-5.

Concentrations and associated chemical properties (see below) are available upon request for all report species.

Calculation of chemical parameters

Gas-phase mass spectrometers measure individual ions with a known molecular formula, while the TD-AMS provides bulk measurements of chemical properties. To explore chemical evolution, volatility must be inferred from molecular composition and vice-versa. Interconversion between c^* and n_C is based on previously published relationships.[60] OS_C is calculated from elemental composition.[41]

Lifetime against atmospheric oxidation for a compound, *i*, is calculated from its rate constant for reaction with OH as $\tau_{ox,i} = \left(k_{OH,i}\overline{[\mathrm{OH}]}\right)^{-1}$ assuming an average OH concentration of 2×10^6 molec cm^{-3}: OH rate constants for known compounds (those labeled in Figures 1-2) are obtained from the NIST Chemical Kinetics Database.[44] Rate constants for unidentified ions are calculated from molecular formula as described by Donahue and co-workers,[45] which spans an atmospheric lifetime of 13 hours for small (high-volatility) gases to ~2 hours for larger (IVOC) gases. Lifetime of unmeasured mass is estimated from its time dependence (~4 hours, Figure S10). Carbon is assumed to be lost from the particle phase with a lifetime of 69 days, as determined by Kroll and co-workers,[46] the conclusions in this work are insensitive to uncertainties in this value.

Uncertainty in carbon closure

Most uncertainties in all instrument calibrations are uncorrelated, so total uncertainty is calculated by adding in quadrature the uncertainty in each ion concentration. The largest source of uncertainty in the total measured concentration is in the calibration of the I^- CIMS, which in this work is ~60% for total carbon concentration (see Supplementary Information Section S4), though expected to be reduced to 20% in future work. The other main source of uncertainty in this work is the predicted bias in PTR measurements caused by the loss of carbon as neutral fragments in the mass spectrometer. Spectra of oxygenated and non-oxygenated compounds previously published[61–64] and measured as part of this work demonstrate that compounds containing more than a few carbon atoms can lose 20% of their carbon as neutral fragments (Tables S1,2 in Supplementary Information Section S5). The consequent predicted underestimation of carbon measured as unknown PTR ions is represented in the asymmetry of the uncertainty estimate. Fragmentation during analysis is also expected to somewhat bias the chemical characterization of the product mixture toward ions with lower carbon numbers. This bias cannot explain the observed decrease in n_C, as this trend is also observed in the I^- CIMS, which does not undergo increased fragmentation with increasing oxidation.

Gas-particle-wall partitioning

Deposition of vapors to the walls was modeled as equilibrium gas-particle-wall partitioning of the observed carbon volatility distribution using parameters to match the conditions of these experiments, using a similar approach to that of La and coworkers.[65] Details of this approach are provided in the Supplementary Information (Section S6). Briefly, the fraction of a volatility bin expected to be on the wall was modeled as a function of equilibration time with parameterized competition between, gas-wall partitioning, gas-particle partitioning, and reaction with OH to form a gas-phase product that does not partition. Time evolution of carbon on walls was simulated by modeled phase partitioning of the observed time-evolving volatility distribution of carbon.

References

1. Sillman, S. The relation between ozone, NOx and hydrocarbons in urban and polluted rural environments. *Atmos. Environ.* **33,** 1821–1845 (1999).
2. Atkinson, R. Atmospheric chemistry of VOCs and NO(x). *Atmos. Environ.* **34,** 2063–2101 (2000).
3. Lelieveld, J., Gromov, S., Pozzer, A. & Taraborrelli, D. Global tropospheric hydroxyl distribution,

budget and reactivity. *Atmos. Chem. Phys.* **16,** 12477–12493 (2016).

4. Yang, Y. *et al.* Towards a quantitative understanding of total OH reactivity: A review. *Atmos. Environ.* **134,** 147–161 (2016).

5. Zhang, Q. *et al.* Ubiquity and dominance of oxygenated species in organic aerosols in anthropogenically-influenced Northern Hemisphere midlatitudes. *Geophys. Res. Lett.* **34,** 1–6 (2007).

6. Jimenez, J.-L. *et al.* Evolution of Organic Aerosols in the Atmosphere. *Science (80-.).* **326,** 1525–1529 (2009).

7. Aumont, B., Szopa, S. & Madronich, S. Modelling the evolution of organic carbon during its gas-phase tropospheric oxidation: development of an explicit model based on a self generating approach. *Atmos. Chem. Phys. Discuss.* **5,** 703–754 (2005).

8. Kroll, J. H. & Seinfeld, J. H. Chemistry of secondary organic aerosol: Formation and evolution of low-volatility organics in the atmosphere. *Atmos. Environ.* **42,** 3593–3624 (2008).

9. Cappa, C. D. & Wilson, K. R. Multi-generation gas-phase oxidation, equilibrium partitioning, and the formation and evolution of secondary organic aerosol. *Atmos. Chem. Phys.* **12,** 9505–9528 (2012).

10. Donahue, N. M., Kroll, J. H., Pandis, S. N. & Robinson, A. L. A two-dimensional volatility basis set-Part 2: Diagnostics of organic-aerosol evolution. *Atmos. Chem. Phys.* **12,** 615–634 (2012).

11. Goldstein, A. H. & Galbally, I. Known and Unexplored Organic Constituents in the Earth's Atmosphere. *Environ. Sci. Technol.* **41,** 1514–1521 (2007).

12. Calvert, J. G., Derwent, R. G., Orlando, J. J., Tyndall, G. S. & Wallington, T. J. *Mechanisms of Atmospheric Oxidation of the Alkanes*. (Oxford University Press, 2007).

13. Lee, A. *et al.* Gas-phase products and secondary aerosol yields from the photooxidation of 16 different terpenes. *J. Geophys. Res. Atmos.* **111,** 1–25 (2006).

14. Lee, A. *et al.* Gas-phase products and secondary aerosol yields from the ozonolysis of ten different terpenes. *J. Geophys. Res. Atmos.* **111,** 1–18 (2006).

15. Zhang, X. *et al.* Influence of vapor wall loss in laboratory chambers on yields of secondary organic aerosol. *Proc. Natl. Acad. Sci. U. S. A.* **111,** 1–6 (2014).

16. Robinson, A. L. *et al.* Rethinking Organic Aerosols: Semivolatile Emissions and Photochemical Aging. *Science (80-.).* **315,** 1259–1262 (2007).

17. Isaacman-VanWertz, G. *et al.* Using advanced mass spectrometry techniques to fully characterize atmospheric organic carbon: current capabilities and remaining gaps. *Faraday Discuss.* **accepted,** (2017).

18. Decarlo, P. F. *et al.* Field-Deployable, High-Resolution, Time-of-Flight Aerosol Mass Spectrometer. *Anal. Chem.* **78,** 8281–8289 (2006).

19. Graus, M., M??ller, M. & Hansel, A. High resolution PTR-TOF: Quantification and Formula Confirmation of VOC in Real Time. *J. Am. Soc. Mass Spectrom.* **21,** 1037–1044 (2010).

20. Jordan, A. *et al.* A high resolution and high sensitivity proton-transfer-reaction time-of-flight mass

spectrometer (PTR-TOF-MS). *Int. J. Mass Spectrom.* **286,** 122–128 (2009).

21. Aljawhary, D., Lee, A. K. Y. & Abbatt, J. P. D. High-resolution chemical ionization mass spectrometry (ToF-CIMS): Application to study SOA composition and processing. *Atmos. Meas. Tech.* **6,** 3211–3224 (2013).

22. Jokinen, T. *et al.* Atmospheric sulphuric acid and neutral cluster measurements using CI-APi-TOF. *Atmos. Chem. Phys.* **12,** 4117–4125 (2012).

23. Krechmer, J. E. *et al.* Formation of Low Volatility Organic Compounds and Secondary Organic Aerosol from Isoprene Hydroxyhydroperoxide Low-NO Oxidation. *Environ. Sci. Technol.* **49,** 10330–10339 (2015).

24. Lee, B. H. *et al.* An Iodide-Adduct High-Resolution Time-of-Flight Chemical- Ionization Mass Spectrometer: Application to Atmospheric Inorganic and Organic Compounds. *Environ. Sci. Technol.* **48,** 6309–6317 (2014).

25. Lopez-Hilfiker, F. D. *et al.* Constraining the sensitivity of iodide adduct chemical ionization mass spectrometry to multifunctional organic molecules using the collision limit and thermodynamic stability of iodide ion adducts. *Atmos. Meas. Tech.* **9,** 1505–1512 (2016).

26. Eddingsaas, N. C. *et al.* α-pinene photooxidation under controlled chemical conditions-Part 1: gas-phase composition in low-and high-NO x environments. *Atmos. Chem. Phys.* **12,** 6489–6504 (2012).

27. Eddingsaas, N. C. *et al.* α-pinene photooxidation under controlled chemical conditions-Part 2: SOA yield and composition in low-and high-NO x environments. *Atmos. Chem. Phys.* **12,** 7413–7427 (2012).

28. Capouet, M., Peeters, J., Nozière, B. & Müller, J.-F. Alpha-pinene oxidation by OH: simulations of laboratory experiments. *Atmos. Chem. Phys. Discuss.* **4,** 4039–4103 (2004).

29. Pathak, R. K., Stanier, C. O., Donahue, N. M. & Pandis, S. N. Ozonolysis of a-pinene at atmospherically relevant concentrations: Temperature dependence of aerosol mass fractions (yields). *J. Geophys. Res. Atmos.* **112,** 1–8 (2007).

30. Jaoui, M. *et al.* Formation of secondary organic aerosol from irradiated α -pinene/toluene/NO x mixtures and the effect of isoprene and sulfur dioxide. *J. Geophys. Res.* **113,** D09303 (2008).

31. Donahue, N. M. *et al.* Aging of biogenic secondary organic aerosol via gas-phase OH radical reactions. *Proc. Natl. Acad. Sci. U. S. A.* **109,** 13503–13508 (2012).

32. Hatakeyama, S., Ohno, M., Weng, J., Takagi, H. & Akimoto, H. Mechanism for the formation of gaseous and particulate products from ozone-cycloalkene reactions in air. *Environ. Sci. Technol.* **21,** 52–57 (1987).

33. Ehn, M. *et al.* Composition and temporal behavior of ambient ions in the boreal forest. *Atmos. Chem. Phys.* **10,** 8513–8530 (2010).

34. Hodshire, A. L. *et al.* Multiple new-particle growth pathways observed at the US DOE Southern Great Plains field site. *Atmos. Chem. Phys.* **16,** 9321–9348 (2016).

35. Ehn, M. *et al.* A large source of low-volatility secondary organic aerosol. *Nature* **506,** 476–479 (2014).

36. Nah, T. *et al.* Influence of seed aerosol surface area and oxidation rate on vapor wall deposition and SOA mass yields: A case study with α-pinene ozonolysis. *Atmos. Chem. Phys.* **16,** 9361–9379 (2016).

37. Trump, E. R., Epstein, S. A., Riipinen, I. & Donahue, N. M. Wall effects in smog chamber experiments: A model study. *Aerosol Sci. Technol.* **50,** 1180–1200 (2016).

38. Ye, P. *et al.* Vapor wall loss of semi-volatile organic compounds in a Teflon chamber. *Aerosol Sci. Technol.* **50,** 0 (2016).

39. Nozière, B., Barnes, I. & Becker, K.-H. Product study and mechanisms of the reactions of α-pinene and of pinonaldehyde with OH radicals. *J. Geophys. Res. Atmos.* **104,** 23645–23656 (1999).

40. Iyer, S., Lopez-Hilfiker, F., Lee, B. H., Thornton, J. A. & Kurtén, T. Modeling the Detection of Organic and Inorganic Compounds Using Iodide-Based Chemical Ionization. *J. Phys. Chem. A* **120,** 576–587 (2016).

41. Kroll, J. H. *et al.* Carbon oxidation state as a metric for describing the chemistry of atmospheric organic aerosol. *Nat. Chem.* **3,** 133–139 (2011).

42. Donahue, N. M., Epstein, S. A., Pandis, S. N. & Robinson, A. L. A two-dimensional volatility basis set: 1. organic-aerosol mixing thermodynamics. *Atmos. Chem. Phys.* **11,** 3303–3318 (2011).

43. Lee, B. H. *et al.* Highly functionalized organic nitrates in the southeast United States: Contribution to secondary organic aerosol and reactive nitrogen budgets. *Proc. Natl. Acad. Sci. U. S. A.* **113,** 1516–1521 (2016).

44. Manion, J. A. *et al. NIST Chemical Kinetics Database, NIST Standard Reference Database 17, Version 7.0 (Web Version), Release 1.6.8, Data version 2015.12*. (National Institute of Standards and Technology, 2015).

45. Donahue, N. M. *et al.* Why do organic aerosols exist? Understanding aerosol lifetimes using the two-dimensional volatility basis set. *Environ. Chem.* **10,** 151–157 (2013).

46. Kroll, J. H., Lim, C. Y., Kessler, S. H. & Wilson, K. R. Heterogeneous Oxidation of Atmospheric Organic Aerosol: Kinetics of Changes to the Amount and Oxidation State of Particle-Phase Organic Carbon. *J. Phys. Chem. A* **119,** 10767–10783 (2015).

47. Dixon-Lewis, G. Flames Structure and Flame Reaction Kinetics VII. Reactions of Traces of Heavy Water, Deuterium and Carbon Dioxide added to rich Hydrogen + Nitrogen + Oxygen Flames. *Proc. R. Soc. London A* **330,** (1972).

48. Raff, J. D., Stevens, P. S. & Hites, R. A. Relative rate and product studies of the OH - Acetone reaction. *J. Phys. Chem. A* **108,** 4728–4735 (2005).

49. Palm, B. B. *et al.* In situ secondary organic aerosol formation from ambient pine forest air using an oxidation flow reactor. *Atmos. Chem. Phys.* **16,** 2943–2970 (2016).

50. Chan, A. W. H. *et al.* Speciated measurements of semivolatile and intermediate volatility organic compounds (S/IVOCs) in a pine forest during BEACHON-RoMBAS 2011. *Atmos. Chem. Phys.* **16,** 1187–1205 (2016).

51. Tkacik, D. S., Presto, A. A., Donahue, N. M. & Robinson, A. L. Secondary organic aerosol formation from intermediate-volatility organic compounds: Cyclic, linear, and branched alkanes. *Environ.*

Sci. Technol. **46,** 8773–8781 (2012).

52. Park, J.-H. *et al.* Active Atmosphere-Ecosystem Exchange of the Vast Majority of Detected Volatile Organic Compounds. *Science (80-.).* **341,** 643–648 (2013).

53. Nguyen, T. B. *et al.* Rapid deposition of oxidized biogenic compounds to a temperate forest. *Proc. Natl. Acad. Sci. U. S. A.* **112,** E392-401 (2015).

54. Wolfe, G. M. *et al.* Formaldehyde production from isoprene oxidation across NOx regimes. *Atmos. Chem. Phys.* **16,** 2597–2610 (2016).

55. Warneke, C. *et al.* Photochemical aging of volatile organic compounds in the Los Angeles basin: Weekday-weekend effect. *J. Geophys. Res. Atmos.* **118,** 5018–5028 (2013).

56. Hunter, J. F., Carrasquillo, A. J., Daumit, K. E. & Kroll, J. H. Secondary organic aerosol formation from acyclic, monocyclic, and polycyclic alkanes. *Environ. Sci. Technol.* **48,** 10227–10234 (2014).

57. Faulhaber, A. E. *et al.* Characterization of a thermodenuder-particle beam mass spectrometer system for the study of organic aerosol volatility and composition. *Atmos. Meas. Tech.* **2,** 15–31 (2009).

58. McManus, J. B. *et al.* Pulsed quantum cascade laser instrument with compact design for rapid, high sensitivity measurements of trace gases in air. *Appl. Phys. B Lasers Opt.* **92,** 387–392 (2008).

59. Lopez-Hilfiker, F. D. *et al.* A novel method for online analysis of gas and particle composition: Description and evaluation of a filter inlet for gases and AEROsols (FIGAERO). *Atmos. Meas. Tech.* **7,** 983–1001 (2014).

60. Daumit, K. E., Kessler, S. H. & Kroll, J. H. Average chemical properties and potential formation pathways of highly oxidized organic aerosol. *Faraday Discuss.* **165,** 181–202 (2013).

61. Tani, A., Hayward, S. & Hewitt, C. N. Measurement of monoterpenes and related compounds by proton transfer reaction-mass spectrometry (PTR-MS). *Int. J. Mass Spectrom.* **223–224,** 561–578 (2003).

62. Buhr, K., Van Ruth, S. & Delahunty, C. Analysis of volatile flavour compounds by Proton Transfer Reaction-Mass Spectrometry: Fragmentation patterns and discrimination between isobaric and isomeric compounds. *Int. J. Mass Spectrom.* **221,** 1–7 (2002).

63. Klein, F. *et al.* Characterization of Gas-Phase Organics Using Proton Transfer Reaction Time-of-Flight Mass Spectrometry: Cooking Emissions. *Environ. Sci. Technol.* **50,** 1243–1250 (2016).

64. Steitz, B. Experimental determination of the partitioning coefficient of nopinone as a marker substance in organic aerosol. (Bergischen Universitat Wuppertal, 2012).

65. La, Y. S. *et al.* Impact of chamber wall loss of gaseous organic compounds on secondary organic aerosol formation: Explicit modeling of SOA formation from alkane and alkene oxidation. *Atmos. Chem. Phys.* **16,** 1417–1431 (2016).

Acknowledgements

We would like to thank Harald Stark for insights into correcting for mass-dependent transmission in the I^- CIMS calibration, Jose-Luis Jimenez for valuable discussions regarding vapor wall loss, and Laura Wattenberg for the inspiration for the stacked plot approach to visualizing these data. This work was supported in large part by NSF Postdoctoral Research Fellowship program (AGS-PRF 1433432), with additional support provided by the Atmospheric Chemistry Program of the U.S. National Science Foundation under grants AGS-1536939, AGS-1537446 and AGS- 1536551. D. A. Knopf acknowledges support from the National Science Foundation grant AGS-1446286.

Author Contribution

GIVW designed, organized, and coordinated the experiments, and assisted in the operation and data analysis of the I^- CIMS, TD-AMS, and SMPS, with support, oversight, contribution of materials, and significant collaboration from JHK. PM led the operation and data analysis of the NO_3^- CIMS and assisted in the operation of the I^- CIMS. REO, CL, and JPL assistant in the operation of the reactor chamber, TD-AMS, and SMPS. JAM developed and implemented the vapor wall loss model. JFH provided guidance on the synthesis of multiple complex datasets into unified frameworks. JBN led the operation and data analysis of the I^- CIMS. MRC contributed to the interpretation and calibration of I^- and NO_3^- CIMS data. PKM, CA, and AHG led the operation, and data analysis and interpretation of the PTR-MS. JRR and STH led the operation, and data analysis and interpretation of the TILDASs. TBO, ATL, JTJ, and DRW assisted in the analysis and interpretation of all CIMS data, and contributed to the scientific understanding of the observed chemical changes and chamber operation. HS contributed the method for transmission corrections in the calibration of I^- CIMS data. LS and DAK contributed the PTR-MS instrument, led its installation, and assisted in its operation.

Competing Financial Interests

The authors declare no competing financial interests.

Materials & Correspondence

All correspondence should be addressed to Prof. Gabriel Isaacman-VanWertz at ivw@vt.edu or Prof. Jesse Kroll at jhkroll@mit.edu .